ACS OMEGA

Open Access

http://pubs.acs.org/journal/acsodf

Article

New Pyrazole-Clubbed Pyrimidine or Pyrazoline Hybrids as Anti-Methicillin-Resistant *Staphylococcus aureus* Agents: Design, Synthesis, *In Vitro* and *In Vivo* Evaluation, and Molecular Modeling Simulation

Basem Mansour,* Magda A. El-Sherbeny, Fatmah A. M. Al-Omary, Sameh Saber, Heba A. Ramadan, Ahmed M. El-Baz, Ahmed A. E. Mourad, and Naglaa I. Abdel-Aziz

Cite This: *ACS Omega* 2023, 8, 44250−44264

Read Online

ACCESS | Metrics & More | Article Recommendations | Supporting Information

ABSTRACT: Two hybrid series of pyrazole-clubbed pyrimidines **5a−c** and pyrazole-clubbed pyrazoline compounds **6a,b** and **7** were designed as attractive scaffolds to be investigated *in vitro* and *in vivo* for antibacterial activity against methicillin-resistant *Staphylococcus aureus* (MRSA) and *Pseudomonas aeruginosa*. From the results of the *in vitro* antibacterial screening, compound **5c** showed excellent activity (minimal inhibitory concentration, MIC = 521 μM) when compared with that of the reference antibiotic levofloxacin (MIC = 346 μM). The inhibition of the target dihydrofolate reductase (DHFR) enzyme by compounds **4** and **5a−c** (IC_{50} = 5.00 ± 0.23, 4.20 ± 0.20, 4.10 ± 0.19, and 4.00 ± 0.18 μM, respectively) was found to be better than the reference drug trimethoprim (IC_{50} = 5.54 ± 0.28 μM). Molecular modeling simulation results have justified the order of activity of all the newly synthesized compounds as DHFR enzyme inhibitors, and compound **5c** exhibited the best binding profile (−13.6169386 kcal/mol). Hence, the most potent inhibitor of the DHFR enzyme, **5c**, was chosen to be evaluated *in vivo* for its activity in treating MRSA-induced keratitis in rats and that, in turn, significantly (P < 0.0001) reduced infection in rats when compared to MRSA-treated group results.

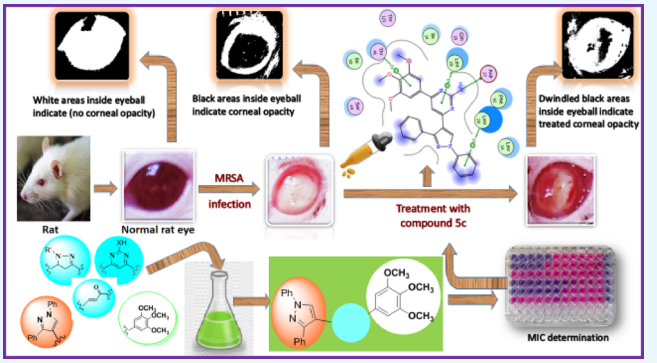

1. INTRODUCTION

The folate biosynthetic pathway has been recognized as a rich source of targets for the development of new antifolate antimicrobial compounds. 5,10-Methylene tetrahydrofolate needs to be synthesized by bacteria and acts as a one-carbon (C1) unit donor for the biosynthesis of deoxythymidine monophosphate, essential in DNA synthesis.[1] It is also used as a C1 unit donor to generate purine nucleotides, histidine, and methionine amino acids.[2] Dihydrofolate reductase (DHFR) is an essential enzyme that catalyzes the reduction of dihydrofolate to tetrahydrofolate, and its inhibition disrupts DNA replication and eventually causes cell death.[3] Pyrimidines, diaminopyrimidines, and related structures are intensively investigated for their DHFR inhibitory activity leading to highly selective and potent anti-MRSA agents.[4,5] Trimethoprim (TMP), 5-(3,4,5-trimethoxybenzyl)pyrimidine-2,4-diamine (**A**), is a well-known antimicrobial agent.[6,7] It inhibits DHFR in bacterial and protozoal cells and has been used clinically since the 1960s (Figure 1).[8] It is usually used alone or in combination with sulfamethoxazole.[9−11] The majority of Gram-positive *Staphylococcus aureus* (*S. aureus*) isolates are susceptible to TMP.[12] However, TMP resistance has increased over the years and therapeutic difficulties have been expressed by methicillin-resistant *S. aureus* (MRSA).[13,14] Such emerging resistance has necessitated the development of active drugs to fight both multidrug-resistant infections and organisms as is often the case of Gram-positive MRSA and Gram-negative *Pseudomonas aeruginosa*. The strategy of developing synthetic antimicrobial compounds mimicking the structure and mechanism of action of conventional antimicrobial agents was reported to optimize the overall properties.[3] In the past, changes at the original TMP core have not been considered as they involve key interactions at the active site of the DHFR enzyme; however, the situation could be otherwise in the mutated enzyme in the resistant strains. Thus, in this work, two series of new TMP analogues have been designed and synthesized using a structure-based approach to improve

Received: September 11, 2023
Revised: October 18, 2023
Accepted: October 20, 2023
Published: November 9, 2023

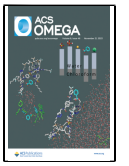

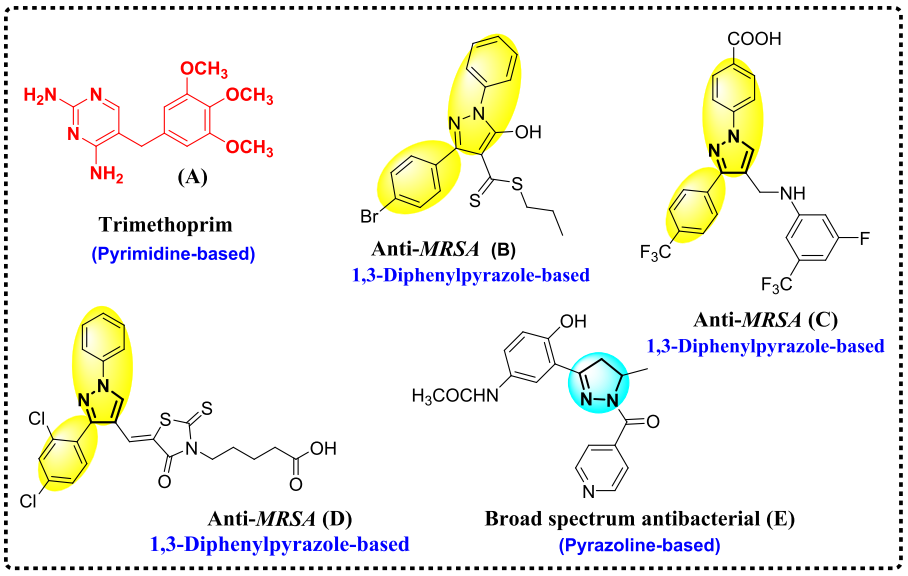

Figure 1. Structures of the reported lead compounds (**A**–**E**).

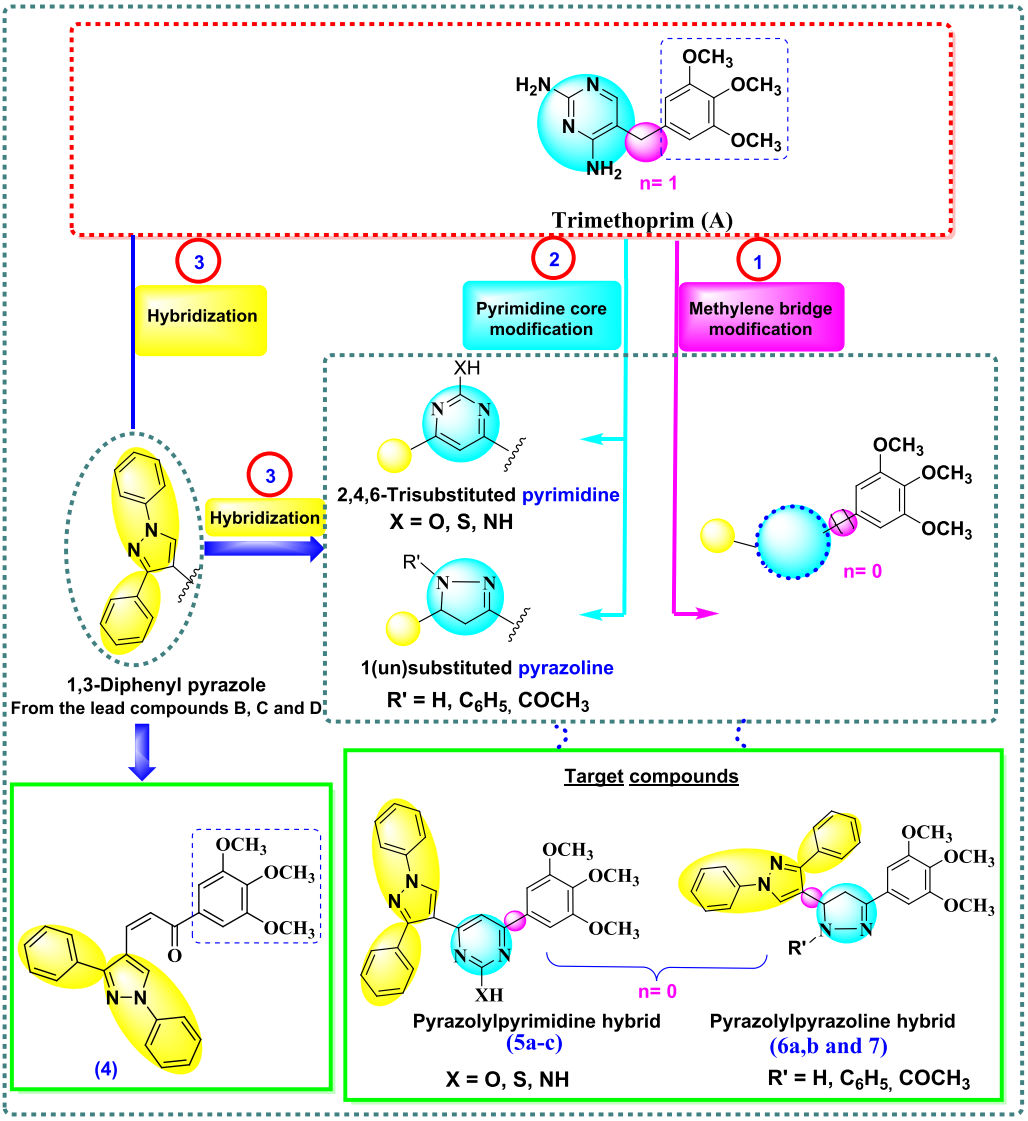

Figure 2. Rationale design of the newly synthesized pyrazole-clubbed pyrimidine or pyrazoline hybrids.

https://doi.org/10.1021/acsomega.3c06936
ACS Omega 2023, 8, 44250−44264

Scheme 1. Synthesis of Diphenylpyrazolyl-Based Chalcone Compound 4, Pyrazolylpyrimidines 5a−c, and Pyrazolylpyrazolines 6a,b and 7

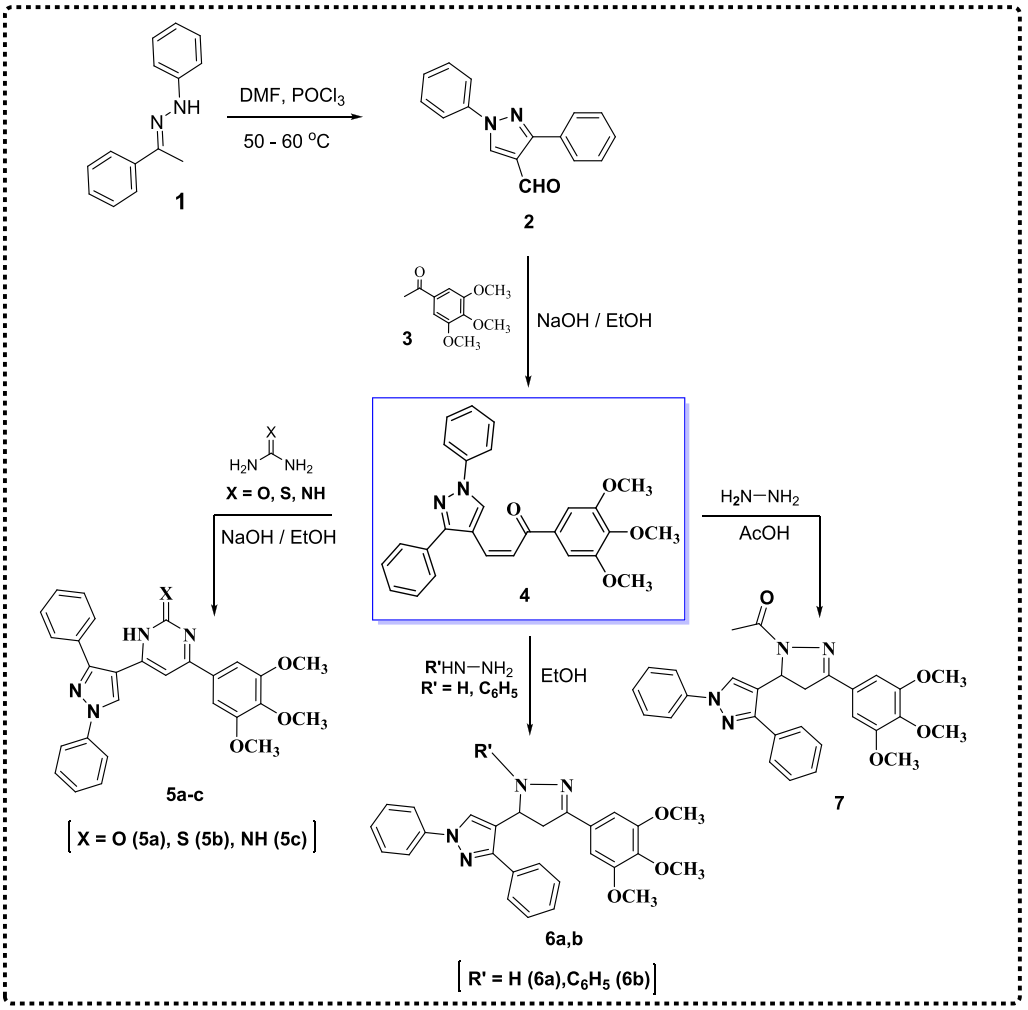

the overall activity and tackle TMP resistance. The literature survey highlighted the 1,3-diphenyl pyrazolyl ring as a pharmacologically attractive scaffold in different antimicrobial agents.[15−18] Additionally, different pyrazole-containing compounds have been demonstrated to possess activity against MRSA particularly 1,3-diphenylpyrazole derivatives as in compounds **B**, **C**, and **D**[19−21] (Figure 1). Hence, our objective was directed to gather two bioactive entities (3,4,5-trimethoxyphenyl and 1,3-diphenyl pyrazolyl) into a hybrid structure (compound **4**) to be the key intermediate for the synthesis of the target compounds. In the first series, the pyrimidine core of TMP with its 2-amino substituent is retained, as in compound **5c**. However, the 2-amino substituent is isosterically replaced by OH or SH groups, as in compounds **5a** and **5b**, respectively. The flexible 3,4,5-trimethoxybenzyl moiety at position 5 of the pyrimidine ring of TMP is modified into a more rigid 3,4,5-trimethoxyphenyl ring via removing the methylene bridge. In the second series (**6a,b** and **7**), the pharmacophoric pyrimidine core is replaced by 1-(un)substituted pyrazoline ring, which was reported to be incorporated in numerous antibacterial agents, either free or conjugated with other heterocyclic rings, as in compound **E**[22] (Figure 1). Also, the methylene bridge was removed in this series. Interestingly, integration and hybridization of the pharmacophoric 1,3-diphenyl pyrazolyl ring in the aforementioned pyrimidine or pyrazoline framework are achieved at position 4. Hence, according to the pharmacophore hybrid approach and via structural modification of the TMP framework, pyrazole-clubbed pyrimidine or pyrazoline hybrids have been synthesized in this work (Figure 2).

The *in vitro* antibacterial activity of the newly synthesized compounds against MRSA and *P. aeruginosa* is investigated, and their potential inhibitory effect on the DHFR enzyme is also determined. Keratitis is an inflammation of the cornea, which is the clear outer layer of the eye. It can be caused by a variety of factors, including infection, injury, allergies, and exposure to certain chemicals or ultraviolet light. Symptoms may include redness, pain, blurred vision, sensitivity to light, and discharge from the eye. Treatment depends on the cause and may include antibiotics, antiviral medications, corticosteroids, lubricating eye drops or ointments, and in some cases surgery.[23−25] Treatment of keratitis caused by MRSA typically involves antibiotics and anti-inflammatory medications. A model of MRSA-induced keratitis has been developed in rats to help in the discovery of more effective treatments that may prevent corneal damage. Accordingly, the most active compounds in the *in vitro* antimicrobial screening were evaluated *in vivo* for their activity in treating keratitis induced by MRSA. In addition, molecular docking methodology was conducted to identify the possible binding interactions

https://doi.org/10.1021/acsomega.3c06936
ACS Omega 2023, 8, 44250−44264

between the target compounds and the DHFR enzyme active site.

2. RESULTS AND DISCUSSION

2.1. Chemistry. The reaction sequences employed for the synthesis of the targeted compounds are outlined in Scheme 1

2.1.1. Synthesis of Compounds 4, 5a−c, 6a,b, and 7 (Scheme 1). Condensation of acetophenone with phenylhydrazine in glacial acetic acid afforded the reported acetophenone phenylhydrazone **1**.[26−28] The later compound was cyclized to pyrazole-4-carbaldehyde **2** in a good yield, after reaction with phosphorus oxychloride and DMF via the well-known Vilsmeier−Haack reaction.[26−28] The new chalcone compound **4** was prepared via Claisen−Schmidt condensation of the pyrazole-4-carbaldehyde **2** with 3′,4′,5′-trimethoxyacetophenone **3** in the presence of ethanolic sodium hydroxide. It is worth noting that the structure of the chalcone intermediate **4** was verified by IR spectroscopy that showed the appearance of the carbonyl stretching vibration of the enone fragment at 1651 cm^{-1}, which was also confirmed by ^{13}C NMR by a signal at δ 188.0 ppm. The ^{1}H NMR spectrum of compound **4** demonstrated characteristic two singlet peaks at δ 3.78 and 3.90 ppm assigned for three protons of the *p*-methoxy group and six protons of the two *m*-methoxy groups, respectively. The alkene protons resonated as two doublets within the aromatic region, which confirmed the formation of the chalcone structure.

The chalcone compound **4** was used as a synthon to synthesize new pyrimidine derivatives **5a−c** by reacting with different nucleophilic reagents such as urea, thiourea, and guanidine in ethanolic sodium hydroxide. The ^{1}H NMR spectra of compounds **5a−c** confirmed the presence of tautomer mixtures with different ratios. For example, in the ^{1}H NMR spectrum of compound **5a,** two singlet peaks resonated at δ 4.48 and δ 8.48 ppm representing the 5-H of pyrimidine-2-one and pyrimidine-2-ol in an 82:18 ratio, respectively. The presence of the keto−enol tautomer mixture, which comprises predominantly the keto form, was also supported by the appearance of two D_2O exchangeable singlets at δ 9.15 and δ 9.35 ppm corresponding to NH and OH protons, respectively, in the ^{1}H NMR spectrum of compound **5a**.

A successful cyclization of the pyrazole-bearing chalcone **4** was achieved through cycloaddition of hydrazine hydrate and phenylhydrazine to give the respective pyrazole−pyrazoline derivatives **6a** and **6b**, respectively, and the construction of the pyrazoline ring was confirmed by the spectroscopic analysis. For example, the notable feature in the ^{1}H NMR spectrum of compound **6b** was the appearance of geminal−vicinal coupling between Ha and Hb at C-4 and Hc at C-5 of the pyrazoline ring. Ha appeared as a doublet of doublets at 3.44 ppm, which is vicinal to Hc and geminal to Hb with coupling constant values of 4.8 and 12.0 Hz, respectively. In addition, Hb appeared as a doublet of doublets at 4.06 ppm with a $J_{Hb,\ Hc}$ value of 12.0 Hz and $J_{Hb,\ Ha}$ value of 7.2 Hz. Last, the Hc proton resonated as a doublet of doublets at 5.52 ppm with *J* values of 7.2 and 4.8 Hz. Moreover, 1-acetyl pyrazoline derivative **7** was obtained by the reaction of compound **4** with hydrazine hydrate in the presence of glacial acetic acid according to the proposed mechanism illustrated in Figure 3.[29]

2.2. Biological Screening. *2.2.1. In Vitro Antimicrobial Activity. 2.2.1.1. Determination of the Inhibition Zones.* The antimicrobial activity of the target compounds **5a−c**, **6a,b**, and

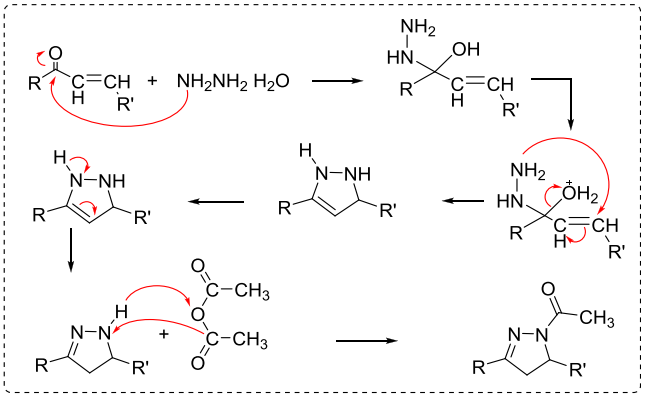

Figure 3. Proposed mechanism for the synthesis of 1-acetyl pyrazoline derivative **7**.

7 was evaluated using the well-known agar diffusion method[30,31] against human pathogenic strains: Gram-positive bacteria MRSA and Gram-negative bacteria *P. aeruginosa* using levofloxacin as a reference drug. levofloxacin is an antibiotic from the fluoroquinolone class and belongs to the third generation, while ofloxacin is an antibiotic from the same class and belongs to the second generation. Therefore, levofloxacin was chosen because it is more effective and potent against MRSA and other bacteria than ofloxacin.[32−34] The inhibition zone (IZ) was measured in millimeters, and the results are summarized in Table 1.

2.2.1.2. Quantitative Assay for Determination of the Minimal Inhibitory Concentration (MIC). Compounds **5a−c** that showed significant growth inhibition zones in the agar diffusion assay, IZ ≥ 18 mm, were chosen to be subjected to a quantitative assay to determine their MIC, which is defined as the lowest concentration at which no visible growth is observed using the microdilution method.

Resazurin-Based 96-Well Plate Microdilution Method. This is an enhanced microdilution method through the addition of the Resazurin redox dye, and it was performed as proposed by the Clinical and Laboratory Standards Institute (CLSI)[35,36] and interpreted using its guidelines.

The active bacterial cells can reduce the nonfluorescent Resazurin (blue) to the fluorescent Resorufin (pink), as shown in Figure 4,[36] and this can be used as an indicator of either bacterial growth (pink color) or inhibition of bacterial growth (blue color). So, according to the CLSI recommendation, the color change can be used to measure the MICs of the tested compounds through the microdilution assay, as shown in Figure 5 and Table 2.

From the *in vitro* antibacterial studies, we can conclude that the synthesized compounds displayed variable inhibitory effects on the growth of the investigated bacterial strains with IZ diameters ranging from 6 to 28 mm. It turned out that all the tested compounds showed greater activity against Gram-positive bacteria represented by MRSA compared to Gram-negative bacteria represented by *P. aeruginosa*. Significant antimicrobial activity was observed for the tested diphenylpyrazolyl-based chalcone **4** with IZ diameters of 17 and 15 mm against MRSA and *P. aeruginosa*, respectively.

Cyclization of compound **4** into the corresponding pyrimidine derivatives **5a−c** resulted in a significant increase in the inhibition potency against both MRSA and *P. aeruginosa*. Among this pyrazole-clubbed pyrimidine series, compound **5c** exhibited the most promising antimicrobial activity against

https://doi.org/10.1021/acsomega.3c06936
ACS Omega 2023, 8, 44250−44264

Table 1. Antimicrobial Activity of Target Compounds Using the Agar Diffusion Method

		IZ (mm)							
	tested bacteria	4	5a	5b	5c	6a	6b	7	levofloxacin
1	MRSA(Gram-positive)	17	25	23	**28**	15	6	11	31
2	P. aeruginosa (Gram-negative)	15	22	20	**24**	6	0	0	27

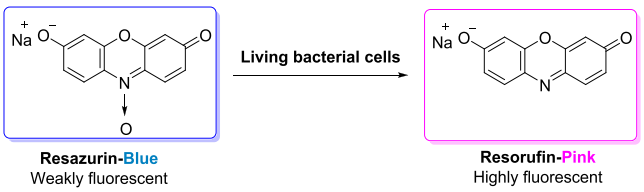

Figure 4. Reduction of Resazurin into Resorufin by living bacteria.

MRSA with the largest zone of inhibition = 28 mm and the lowest MIC = 521 μM as compared to the reference drug levofloxacin (IZ = 31 mm and MIC = 346 μM). Moreover, a zone of inhibition = 24 mm was exhibited by compound **5c** against *P. aeruginosa* with MIC = 2085 μM, which is comparable to levofloxacin (IZ = 27 mm and MIC = 1384 μM).

Also, compounds **5a** and **5b** showed promising antibacterial activity against MRSA with IZ = 25 and 23 mm and MIC = 2081 and 1007 μM, respectively. In addition, the latter compounds exhibited good activity against *P. aeruginosa*, as revealed from the calculated IZ and MIC values. A little decrease in the activity of compounds **5a** and **5b** in comparison with compound **5c** was noticed, and this is possibly attributed to the isosteric replacement of the NH substituent at position 2 of the pyrimidine ring in compound **5c** with OH and SH in compounds **5a** and **5b**, respectively. On the other hand, cyclization of the chalcone compound **4** into the corresponding pyrazoline derivatives **6a,b** and **7** showed a relative decrease in the antibacterial activity particularly against the Gram-negative strain, *P. aeruginosa*. The results for this

Table 2. Determination of the MIC of the Tested Compounds 5a−c by the Resazurin-Aided Microdilution Method

		MIC of the tested compounds (μM)			
	tested bacteria	5a	5b	5c	levofloxacin
1	MRSA(Gram-negative)	2081	1007	521	346
2	P. aeruginosa(Gram-negative)	8324	4027	2085	1384

pyrazole-clubbed pyrazoline series showed that the antibacterial activity was significantly influenced by the substituent at the N of the pyrazoline ring. Hence, the unsubstituted compound **6a** showed more inhibitory activity against Gram-positive bacterial strain, MRSA, followed by compound **7** with an acetyl substituent and then compound **6b** with a more lipophilic bulky phenyl substituent. Regarding the activity against *P. aeruginosa*, Compound **6a** exhibited weak activity with IZ = 6 mm while compounds **6b** and **7** had no detectable activity.

2.2.2. Dihydrofolate Reductase (DHFR) Inhibition Assay. As an attempt to reveal whether the antibacterial activity of the proposed compounds was related to the inhibition of the DHFR enzyme, an *in vitro* DHFR inhibition assay was performed. All of the synthesized compounds **4**, **5a−c**, **6a,b**, and **7** were subjected to the DHFR inhibition evaluation assay adopting the reported procedures using TMP as a reference drug. IC_{50} values in micromolar concentrations of the tested compounds were calculated and are listed in Table 3 and graphically represented in Figure 6. Compounds **4** and **5a−c**

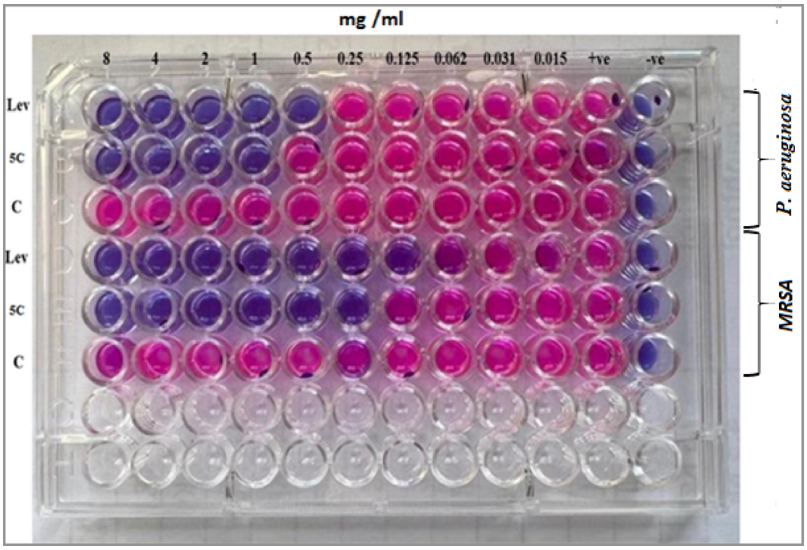

Figure 5. Determination of the MIC of compound **5c** using the Resazurin-based 96-well plate microdilution method. −ve:sterility control in well 12 (broth + Resazurin) shows the natural blue color of Resazurin to confirm that no contamination occurred while preparing the plate. +ve:control without the drug in well 11 (broth + bacteria (*P. aeruginosa* or MRSA) + Resazurin) shows change of the natural color of Resazurin into the reduced form color (pink). Lev.: reference drug levofloxacin as a positive control in serial dilutions in wells 1−10. **5c**: test compound in serial dilutions in wells 1−10. C: Negative control containing DMSO instead of the test compound.

https://doi.org/10.1021/acsomega.3c06936
ACS Omega 2023, 8, 44250−44264

Table 3. Results of the *In Vitro* DHFR Inhibition Assay and Docking Interaction Energy

comp. no.	IC_{50} (μM)[a] DHFR inhibition	docking interaction energy (kcal/mol)
4	5.00 ± 0.23	−11.8926764
5a	4.20 ± 0.20	−13.0764761
5b	4.10 ± 0.19	−12.7614536
5c	4.00 ± 0.18	−13.6169386
6a	5.56 ± 0.27	−12.004714
6b	6.45 ± 0.31	−10.8985271
7	6.70 ± 0.31	−11.0561876
TMP	5.54 ± 0.28	−10.6276875

[a]IC_{50} (μM): Expressed as mean ± SD.

proved to be the most active DHFR inhibitors among the tested compounds with IC_{50} values of 5.00 ± 0.23, 4.20 ± 0.20, 4.10 ± 0.19, and 4.00 ± 0.18 μM, respectively, which are better than that of the standard drug (IC_{50} = 5.54 ± 0.28 μM). Moreover, compound **6a** showed nearly comparable activity with TMP, as revealed from its IC_{50} = 5.56 ± 0.27 μM. However, compounds **6b** and **7** revealed to be the least inhibitors toward DHFR in comparison to TMP with IC_{50} values of 6.45 ± 0.31 and 6.70 ± 0.31 μM, respectively.

2.2.3. In Vivo Antimicrobial Activity. From the *in vitro* antimicrobial screening of the newly synthesized compounds, it turned out that compound **5c** showed excellent antimicrobial activity against MRSA with promising inhibition of the DHFR enzyme. Hence, it was chosen to be evaluated *in vivo* for its activity in treating MRSA-induced keratitis in rats.

*2.2.3.1. Effect of the Tested Compound **5c** on the Area % of Corneal Opacity.* The infected eyes were photographed on the third day after infection, and the images were processed with ImageJ 1.52i software (NIH, Bethesda, MD, USA). The black areas inside the eyeballs in the ImageJ-processed photographs designate the areas of focal lesions, as shown in Figure 7. The white areas represent the uninfected areas of the eyeballs. Area % of corneal opacity was calculated as a measure of the clinical presentation of corneal MRSA infection. Even when blinded, this method was used to reduce the bias and errors associated with assessing clinical presentation scores by an ophthalmologist.[37]

As a result, more precise determinations are guaranteed. In this regard, keratitis treatment with compound **5c** significantly reduced infection in rats when compared to the MRSA-treated group. This was demonstrated by a significant reduction in the area % of corneal opacity in the **5c** dispersion-treated infected group compared to that of the MRSA group (Figure 8).

*2.2.3.2. Effect of the Tested Compound **5c** on the Inflammation Score.* Our study evaluated the degree of corneal inflammation in three groups: a normal group, MRSA group, and MRSA/**5c** dispersion group. The normal group did not show any signs of corneal inflammation. In contrast, the MRSA group exhibited severe inflammatory cell infiltration and edema, as shown in Figure 9.

On the other hand, the MRSA/**5c** dispersion group showed a significant decrease in inflammation score with mild to moderate inflammatory cell infiltration compared to the MRSA group, as illustrated in Figure 10.

2.3. Molecular Modeling Simulation. Molecular modeling simulation has been conducted to investigate the interactions of our compounds with the TMP binding site in the crystal structure of wild-type *S. aureus* DHFR.

Docking results of compound **4** showed that the conserved amino acid Leu20 formed a trifurcated H-arene bond with the trimethoxylated phenyl ring at one side, pyrazole ring at the middle, and phenyl ring attached at position 3 of the pyrazole ring at the other side of the ligand. Additionally a conspicuous H-bond was constructed between the backbone of the conserved H-bond donor amino acid Gln19 and the H-bond acceptor nitrogen atom at position 2 of the pyrazole ring. Enhanced by the hydrophobic/hydrophilic interactions, the free binding energy scored −11.8926764 kcal/mol (Figure S25).

However, docking results showed that compound **5a** built an H-bond via the hydrogen atom of its hydroxyl group and the side chain of the conserved H-bond acceptor amino acid Ser49. Furthermore, the conserved amino acid Leu28 constructed a characteristic bifurcated H-arene bond with the pyrazole ring and the phenyl ring substituted at its position 1, augmenting the free binding energy up to −13.0764761 kcal/mol (Figure S25).

However, upon docking of compound **5b**, we found that the conserved amino acid Leu20 via its side chain formed a bifurcated H-arene bond with the pyrimidine ring and its trimethoxylated phenyl substituent at position 4 along with the H-bond constructed between thiol hydrogen and the side

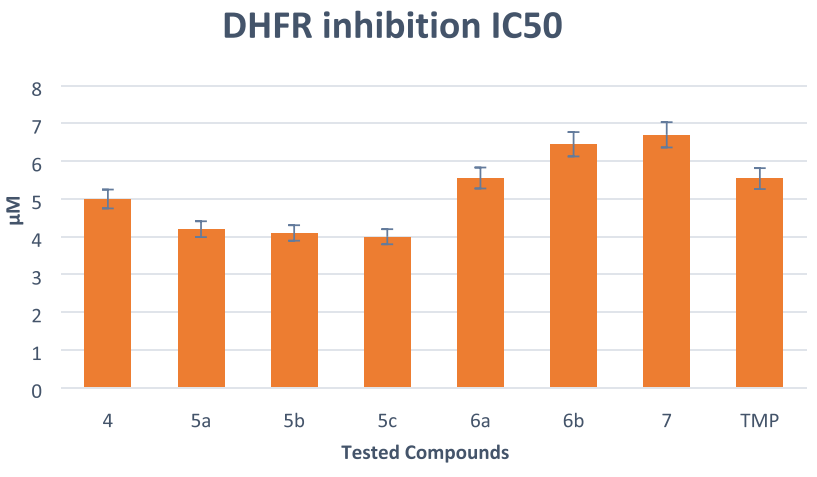

Figure 6. DHFR inhibition chart of the tested compounds versus TMP (reference drug) expressed as IC_{50} (μM).

https://doi.org/10.1021/acsomega.3c06936
ACS Omega 2023, 8, 44250−44264

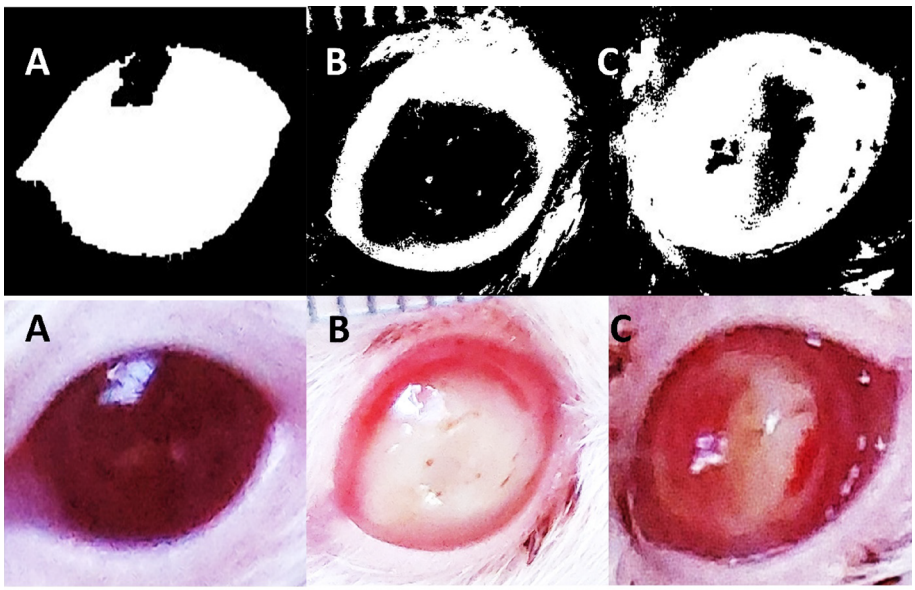

Figure 7. Photographs showing ImageJ-processed images (upper panel) of the (A) normal eye, (B) MRSA infected eye, and (C) MRSA infected eye and treated with compound **5c**. Black areas inside eyeballs indicate corneal opacity as a direct measure of the infection intensity. The lower panel shows unprocessed eyes from different groups.

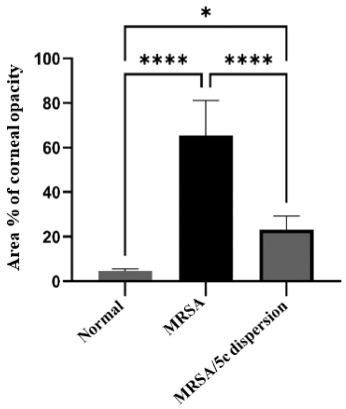

Figure 8. Effect of the compound **5c** dispersion on the area % of corneal opacity as a direct measure of infection intensity. *P < 0.05; ****P < 0.0001 as indicated by the pairwise comparisons.

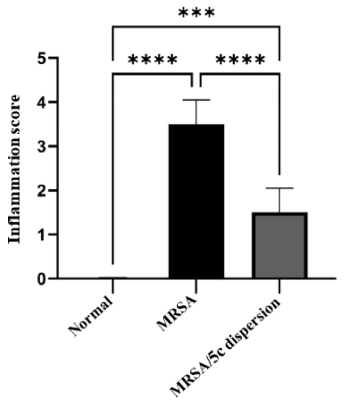

Figure 10. Effect of compound **5c** dispersion on the inflammation score. The MRSA/**5c** dispersion group showed a significant decrease in inflammation score compared to that of the MRSA group. The inflammation score criteria were as follows: 0, no inflammation; 1, minimal inflammation; 2, mild inflammation; 3, moderate inflammation; 4, severe inflammation. Results represent mean ± standard deviation (SD), n = 6 per group. ***p < 0.001, ****p < 0.0001.

chain of conserved acidic amino acid Asp27, enhancing the free binding energy up to −12.7614536 kcal/mol (Figure S25).

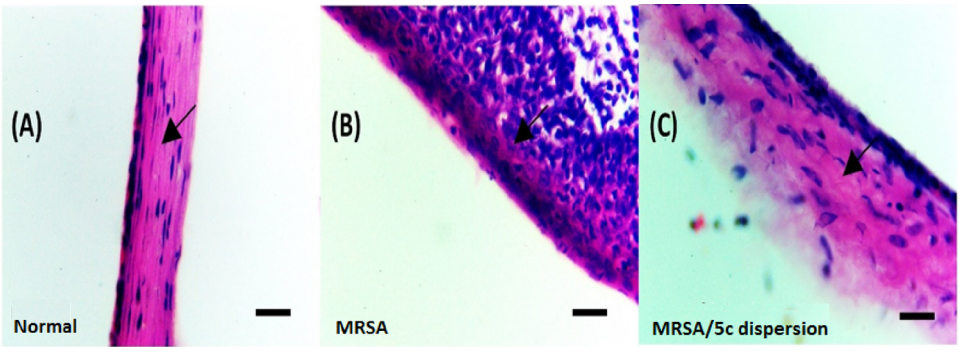

Figure 9. Histological evaluation of corneal inflammation in response to MRSAinfection and **5c** dispersion therapy. Corneal sections were stained with H&E to evaluate the degree of inflammation. (A) The normal group showed no signs of corneal inflammation. (B) The MRSA group exhibited severe inflammatory cell infiltration and edema. (C) The MRSA/**5c** dispersion group showed mild inflammatory cell infiltration compared to the MRSA group. Scale bars = 50 μm.

https://doi.org/10.1021/acsomega.3c06936
ACS Omega 2023, 8, 44250−44264

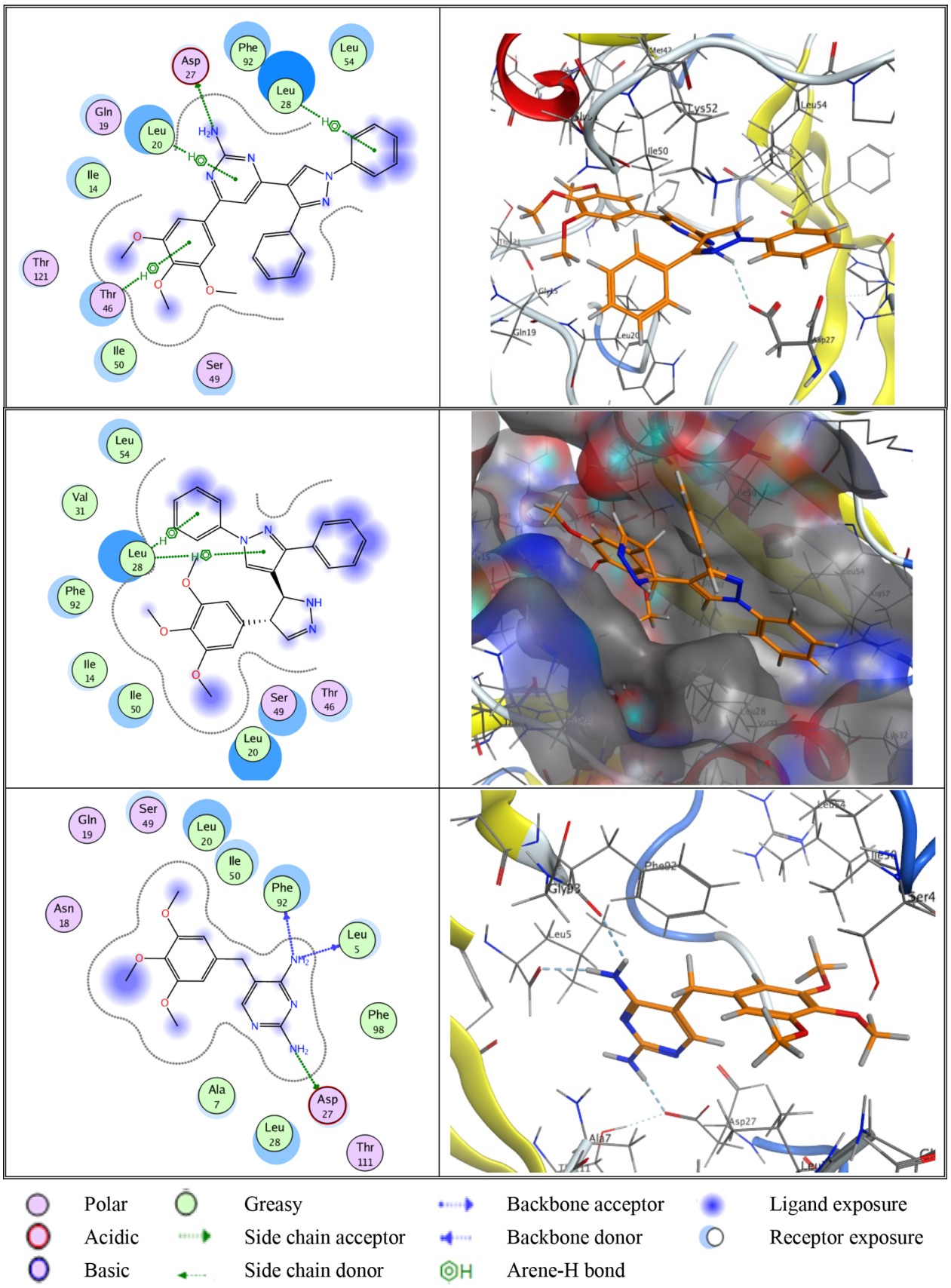

Figure 11. Putative binding modes of compounds **5c** (upper panel), **6a** (middle panel), and TMP (lower panel) with the receptor pocket of TMP (PDB ID: 2w9h).

https://doi.org/10.1021/acsomega.3c06936
ACS Omega 2023, 8, 44250−44264

Even though in the case of the third pyrimidine analogue compound **5c** (Figure 11), a unique binding profile was exhibited. The two teriminals of the ligand, the phenyl ring at position 1 to the pyrazole and the trimethoxylated phenyl, were bonded through two arene-H bonds to the conserved amino acids Leu28 and Thr46, respectively. Meanwhile, at the middle, the pyrimidine ring, in turn, added noticeable fixation of the ligand inside the TMP binding site in the receptor by forming two different types of bonds: the arene-H-bond with Leu20 and H-bond with the H-bond acceptor Asp27. In addition, the recognition of ligands inside the active core is greatly enriched by the markedly observed hydrophobic/hydrophilic interactions from the cyan shadow around Ile14, Gln19, Leu20, Leu28, Thr46, Ser49, Ile50, Leu54, and Phe92 from the receptor side and the blue shadow around the two phenyl rings substituted at positions 1 and 3 of the pyrazole ring, as well as the trimethoxylated phenyl ring and pyrimidine ring with its amino group, from the ligand side. Hence, the free binding energy has achieved −13.6169386 kcal/mol.

On the other hand, docking of compound **6a** (Figure 11) as the first member of bipyarazole analogues revealed that the conserved amino acid Leu28 has established a bifurcated H-arene bond with the pyarzole ring and its phenyl substituent at position 1. The diphenyl rings at positions 1,3 of the pyrazole ring displayed an intense blue shadow around as well as the three methoxy groups from the ligand side, and Leu20, Leu28, Thr46, Ser49, Ile50, Leu54, and Phe92 displayed an intense cyan shadow around, indicating a good hydrophobic/hydrophilic interaction pattern. Eventually, the free binding energy scored −12.004714 kcal/mol.

Although it has the least binding profile, compound **6b** that comprises two 1,3-diphenyl pyrazoline and 1,3-diphenylpyrazole moieties linked at the 3,4′ position of the two heterocyclic rings exhibited superiority of the 1-phenyl-3-(3,4,5-trimethoxyphenyl)-pyrazoline moiety in increasing the stability of the ligand/receptor complex rather than a 1,3-diphenylpyrazole moiety of 4.294. That is to say, in the intact compound structure, the phenyl ring attached to position 2 of the pyrazoline ring formed a bifurcated arene-H-bond with the conserved amino acids Val6 and Ala7, whereas the *p*-methoxy group of the phenyl ring attached to position 5 in the same moiety constructed an H-bond with the backbone of the conserved H-bond donor amino acid Leu24 ending up with a free binding energy of −10.8985271 kcal/mol (Figure S25).

Contrarily, the compound 7 bearing acetyl group at position 2 instead of the phenyl ring as in compound **6b** of the pyrazoline ring showed that the pacemaker for the stability of the ligand/receptor complex is the 1,3-diphenylpyrazole moiety as it established, through its diphenyl wings, two arene-H bonds with Leu28 and Leu20, giving rise to achieving a total score of free binding energy of −11.0561876 kcal/mol (Figure S25).

Scrutinizing TMP (Figure 11), it consists of two moieties: hydrophilic pyrimidine-2,4-diamine and fairly hydrophobic trimethoxyphenyl linked through a methylene linker. The amino group at position 4 of the pyrimidine ring displayed a bifurcated H-bond with the backbones of the conserved H-bond acceptor amino acids Leu5 and Phe92; however, the latter amino group at position 2 formed an H-bond with the side chain of the conserved amino acid Asp27. Moreover, the hydrophobic/hydrophilic interactions improved the overall recognition of the ligand inside the active site leading to a total free binding energy of −10.6276875 kcal/mol.

Noteworthy, all the newly synthesized compounds achieved a higher free binding energy score rather than TMP. In addition, the cyclization of the propenone linker in compound **4** into pyrimidine as a six-membered heterocycle increased the stability of the ligand/receptor complex, while into pyrazoline as a five-membered heterocycle, it decreased that stability. Indubitably, the pyrimidine analogue set (**5a−c**) displayed a better binding profile and affinity toward the TMP binding site over the pyrazoline analogue set (**6a,b** and **7**). However, preserving the amino group in position 2 of the pyrimidine ring (like TMP) as in compound **5c** has presented the best binding profile with a free binding energy of −13.6169386 kcal/mol, even surmounting its isosters OH and SH groups in compounds **5a** and **5b**, respectively. On the other hand, pyrazoline derivative (**6a,b** and **7**) docking results revealed that the order in binding strength was **6a** > **7** > **6b**; that is to say, unsubstitution of pyrazoline is preferable over substitution in general, although substitution with a small group like acetyl as in compound **7** is better than substitution with a bulky group like the phenyl group as in compound **6b**.

3. CONCLUSIONS

With an aim of developing potent antimicrobial agents against the resistant strains MRSA and *P. aeruginosa*, new hybrids of pyrazole−pyrimidine and pyrazole−pyrazoline compounds were synthesized from the starting pyrazole-based chalcone **4** and characterized by IR, ^{1}H NMR, ^{13}C NMR, mass spectroscopy, and elemental analyses. All the target compounds were screened for their *in vitro* antimicrobial activity, and their MIC values were determined against the tested microorganisms in comparison with levofloxacin. The results suggest that the order of inhibitory activity is scaffold-based and influenced by the substitution pattern. Accordingly, the antimicrobial activity showed by the pyrimidine compounds **5a−c** is greater than those exhibited by the chalcone compound **4** and the last pyrazolines **6a,b** and **7**. Moreover, among the pyrimidine compounds, the NH substituent at position 2 of the pyrimidine ring is more desirable, as observed in the enhanced antibacterial activity of compound **5c**. However, among the pyrazoline compounds, better activity was noticed with the unsubstituted derivative **6a** followed by the *N*-acetyl derivative **7**, while the activity was greatly decreased with a larger substituent as in compound **6b**. High levels of inhibition of the DHFR enzyme were obtained by compounds **4** and **5a−c** with IC_{50} better than the TMP reference drug. The promising active compound **5c** was chosen for further *in vivo* study to evaluate its activity in treating MRSA-induced keratitis in rats, and the results appeared promising. There was a good agreement between the results of the docking study and the DHFR assay. Compound **5c** showed the best MIC values (521 and 2085 μM) among the tested compounds, which is two-thirds the potency of levofloxacin (MIC = 346 and 1384 μM) against MRSA and *P. aeruginosa*, respectively, and its activity in treating keratitis is encouraging. Also, this showed inhibition of DHFR with IC_{50} = 4.00 ± 0.18 μM and scored free binding energy of −13.6169386 kcal/mol in the docking study, which are better than those of TMP (IC_{50} = 5.54 ± 0.28 μM and free binding energy of −10.6276875 kcal/mol). Hence, this pyrazolypyrimidine hybrid skeleton may provide a valuable lead for designing and developing novel antibacterial agents against MRSA.

https://doi.org/10.1021/acsomega.3c06936
ACS Omega 2023, 8, 44250−44264

4. EXPERIMENTAL SECTION

4.1. Chemistry. All chemicals and solvents were reagent grade and used without further purification. Melting points (°C) were recorded using a Stuart melting point apparatus and were uncorrected. IR spectra were recorded on a Shimadzu IR-470 spectrometer (υ' in cm^{-1}) using a KBr disk at Faculty of Pharmacy, Mansoura University, Egypt. ^1H NMR and ^{13}C NMR spectra were recorded on a Jeol spectrometer at 500 and 125 MHz, respectively, in DMSO-d_6 with TMS as the internal standard at Faculty of Science, Mansoura University, Egypt and Bruker spectrometer at 400 and 100 MHz, respectively, in DMSO-d_6 with TMS as the internal standard at Faculty of Pharmacy, Mansoura University, Egypt. The mass spectra were recorded in ESI^+ and ESI^- modes by a Shimadzu LC-MS/MS 8045, Column UPLC RP-18, particle size of 2.1 μm with a flow rate 0.2 mL/min, and mobile phase acetonitrile: water 70%, at Center of Drug Discovery Research and Development, Faculty of Pharmacy, Ain Shams University, Egypt. Elemental analysis was carried out for C, H, and N at the Microanalytical Centre of Cairo University, and they agreed with proposed structures within ±0.4% of the calculated values. Column chromatography was carried out on a Silica Gel G60 (70−230 mesh, ASTM; Merck and 230−400 mesh, Silicycle Inc.). The completion of reactions was monitored using thin layer chromatography (TLC) on Silica Gel G60 F-245 (Merck), and the spots were visualized by U.V. (366, 245 nm). Compounds (*E*)-1-phenyl-2-(1-phenylethylidene)hydrazine (**1**) and 1,3-diphenyl-1*H*-pyrazole-4-carbaldehyde (**2**) were prepared according to the previously reported procedures.[38−40]

*4.1.1. Procedure for the Synthesis of (Z)-3-(1,3-Diphenyl-1H-pyrazol-4-yl)-1-(3,4,5-trimethoxyphenyl)prop-2-en-1-one (**4**).* To a stirred ice-cooled solution of absolute ethanol (12.5 mL) and sodium hydroxide (0.4 g; 10 mmol), 3′,4′,5′-trimethoxyacetophenone **3** (2.1 g; 10 mmol) was added followed by 1,3-diphenyl-1*H*-pyrazole-4-carbaldehyde **2** (2.5 g; 10 mmol). The reaction mixture was vigorously stirred for 3 h, while the temperature was maintained below 25 °C and was left in a refrigerator overnight. The formed precipitate was filtered off and washed with a copious amount of water, washed with ice-cold ethanol (20 mL), dried, and recrystallized from ethanol to afford compound **4**.

Pale yellow crystals, mp 110−112 °C, yield (84%), IR (KBr, ν, cm^{-1}): 3060 (CH-aromatic), 2836−2938 (CH-aliphatic), 1651 (C═O), 1575 (C═N), 1125 (C−O aliphatic ether). ^1H NMR (400 MHz, DMSO-d_6): δ 3.78(s, 3H, *p*-methoxy), 3.90(s, 6H, *m*-methoxy), 7.35(s, 2H, H-2, H-6 trimethoxyphenyl), 7.43(t, 1H, J = 7.2 Hz, H-4′ phenyl) 7.53(t, 1H, J = 7.2 Hz, H-4, *N*-phenyl), 7.60(dt, 4H, J = 7.2 Hz, J = 1.2 Hz, H-3, H-5, H-3′, H-5′), 7.69(d, 3H, J = 6.8 Hz, α-proton-alkene, H-2′, H-6′), 7.78(m, 2H, H-2, H-6), 7.96(d, 1H, J = 7.2 Hz, β-proton-alkene), 9.36(s, 1H, H-pyrazole). ^{13}C NMR (100 MHz, DMSO-d_6): δ 56.7(*m*-methoxy), 60.7(*p*-methoxy), 106.5(C-2, C-6 trimethoxyphenyl), 118.2(C-4 pyrazole), 119.3(C-2, C-6), 121.6(C-4), 127.6(α-C-alkene), 129.0(C-2′, C-6′), 129.3(C-4′), 129.4(C-3′, C-5′), 129.5(C-1 trimethoxyphenyl), 130.2(C-3, C-5), 132.5(C-5 pyrazole), 133.5(C-1′), 134.6(C-1), 139.4(C-4 trimethoxyphenyl), 142.4(β-C alkene), 153.4(C-3, C-5 trimethoxyphenyl), 153.5(C-3 pyrazole), 188.0(C-carbonyl). Anal. Calc. for $C_{27}H_{24}N_2O_4$ (MW; 440.50) calculated %; C: 73.62, H: 5.49, N: 6.36. Found %; C: 73.59, H: 5.51, N: 6.38.

*4.1.2. Procedure for the Synthesis of 6-(1,3-Diphenyl-1H-pyrazol-4-yl)-4-(3,4,5-trimethoxyphenyl)pyrimidine Derivatives **5a−c**.* A mixture of chalcone (4.4 g; 10 mmol) and urea, thiourea, or guanidine (10 mmol) was dissolved in ethanolic sodium hydroxide (10 mL of ethanol, 4 g of NaOH), stirred at room temperature for 2−3 h, and then poured into 400 mL of cold water with continuous stirring for 1 h. The reaction mixture was kept in the refrigerator for 24 h. The precipitate was filtered off, washed using ice-cold 4% aqueous HCl, dried, and recrystallized from ethanol to afford compounds **5a−c.**

*4.1.2.1. 6-(1,3-Diphenyl-1H-pyrazol-4-yl)-4-(3,4,5-trimethoxyphenyl)pyrimidine-2(1H)-one (**5a**).* Beige crystals, mp >300 °C, yield (80%), IR (KBr, ν, cm^{-1}): 3418(NH), 3061 (CH-aromatic), 2853−2923 (CH-aliphatic), 1659 (C═O), 1586 (C═N), 1126 (C−O aliphatic ether). ^1H NMR (500 MHz, DMSO-d_6): δ 3.88(s, 3H, *p*-methoxy), 3.96 (s, 6H, *m*-methoxy), 4.48(s, 1H, 5-H pyrimidine-2(1*H*)-one, 82%), 6.97(s, 2H, 2-H, 6-H trimethoxyphenyl, 18%), 7.06(s, 2H, 2-H, 6-H trimethoxyphenyl, 82%), 7.24(t, 1H, J = 8.0 Hz, H-4′ phenyl), 7.34(t, 1H, J = 7.5 Hz, H-4, *N*-phenyl), 7.41(dt, 4H, J = 8.0 Hz, J = 2.5 Hz, H-3, H-5, H-3′, H-5′), 7.55(d, 2H, J = 7.5 Hz, H-2′, H-6′), 7.74(d, J = 7.5 Hz, 2H, H-2, H-6), 8.30(s, 1H, pyrazole-H), 8.48(s, 1H, 5-H pyrimidine-2-ol, 18%), 9.35(s, 1H, OH exchangeable by D_2O, 18%), 9.15(s, 1H, NH exchangeable by D_2O, 82%). ^{13}C NMR (125 MHz, DMSO-d_6): δ 56.1(*m*-methoxy), 60.6(*p*-methoxy), 106.3(C-2, C-6 trimethoxyphenyl), 109.1(C-5 pyrimidine), 112.9(C-4 pyrazole), 120.4(C-2, C-6), 126.6(C-4), 127.7(C-1 trimethoxyphenyl), 128.1(C-2′, C-6′), 128.9(C-4′), 129.5(C-3′, C-5′), 129.8(C-3, C-5), 131.9(C-3 pyrazole), 133.6(C-1′), 139.8(C-1), 141.2(C-4 trimethoxyphenyl), 150.7(C-5 pyrazole), 153.1(C-3, C-5 trimethoxyphenyl), 156.4 (C═O), 163.5(C-6 pyrimidine), 165.1(C-4 pyrimidine). LC-MS/MS m/z (ESI): 481.15 $[M+H]^+$, 479.20$[M-H]^-$. Anal. Calc. for $C_{28}H_{24}N_4O_4$ (MW; 480.52) calculated %; C: 69.99, H: 5.03, N: 11.66. Found %; C: 70.01, H: 5.06, N: 11.63.

*4.1.2.2. 6-(1,3-Diphenyl-1H-pyrazol-4-yl)-4-(3,4,5-trimethoxyphenyl)pyrimidine-2(1H)-thione (**5b**).* Yellow crystals, mp >300 °C, yield (77%), IR (KBr, ν, cm^{-1}): 3419(NH), 3060 (CH-aromatic), 2851−2926 (CH-aliphatic), 1534 (C═N), 1159 (C═S), 1125 (C−O aliphatic ether). ^1H NMR (400 MHz, DMSO-d_6): δ 3.81(s, 3H, *p*-methoxy), 3.89 (s, 6H, *m*-methoxy), 6.70(s, 1H, 5-H pyrimidine-2(1*H*)thione, 77%), 7.21(s, 2H, 2-H, 6-H trimethoxyphenyl, 23%), 7.34(s, 2H, 2-H, 6-H trimethoxyphenyl, 77%), 7.44(t, 1H, J = 7.2 Hz, H-4′ phenyl), 7.52(t, 1H, J = 7.2 Hz, H-4, *N*-phenyl), 7.58(dt, 4H, J = 7.2 Hz, J = 1.2 Hz, H-3, H-5, H-3′, H-5′), 7.68(d, 2H, J = 6.8 Hz, H-2′, H-6′), 7.79(d, J = 6.8 Hz, 2H, H-2, H-6), 8.66(s, 1H, pyrazole-H), 8.75(s, 1H, 5-H pyrimidine-2-thiol, 23%), 9.35(s, 1H, NH exchangeable by D_2O, 77%), 9.99(s, 1H, SH exchangeable by D_2O, 23%). ^{13}C NMR (100 MHz, DMSO-d_6): δ 56.3(*m*-methoxy), 60.2(*p*-methoxy), 106.0(C-2, C-6 trimethoxyphenyl), 107.8(C-5 pyrimidine), 118.9(C-4 pyrazole), 128.4(C-2, C-6), 128.6(C-4), 128.7(C-1 trimethoxyphenyl), 128.9(C-2′, C-6′), 129.0(C-4′), 129.5(C-3, C-5), 129.8(C-3′, C-5′), 132.9(C-3 pyrazole), 138.9(C-1′), 141.8(C-1), 142.0(C-4 trimethoxyphenyl), 152.7(C-5 pyrazole), 152.9(C-3, C-5 trimethoxyphenyl), 153.1(C-4 pyrimidine), 184.5(C-6 pyrimidine), 187.8 (C═S). Anal. Calc. for $C_{28}H_{24}N_4O_3S$ (MW; 496.59) calculated %; C: 67.72, H: 4.87, N: 11.28. Found %; C: 67.70, H: 4.90, N: 11.25.

https://doi.org/10.1021/acsomega.3c06936
ACS Omega 2023, 8, 44250−44264

*4.1.2.3. 6-(1,3-Diphenyl-1H-pyrazol-4-yl)-4-(3,4,5-trimethoxyphenyl)pyrimidine-2(1H)-imine (**5c**).* Yellow crystals, mp 288−292 °C, yield (87%), IR (KBr, ν, cm^{-1}): 3415(NH), 3062 (CH-aromatic), 2838−2937 (CH-aliphatic), 1587 (C═N), 1336 (C−N stretching aromatic amine), 1127 (C−O aliphatic ether). ^{1}H NMR (400 MHz, DMSO-d_6): δ 3.70(s, 3H, *p*-methoxy), 3.79(s, 6H, *m*-methoxy), 5.26(s, 1H, NH exchangeable by D_2O, 78%), 5.40(s, 2H, NH_2 exchangeable by D_2O, 22%), 6.63(s, 1H, 5-H pyrimidine-2(1*H*)-imine, 78%), 6.96(s, 2H, 2-H, 6-H trimethoxyphenyl, 22%), 7.11(s, 2H, 2-H, 6-H trimethoxyphenyl, 78%), 7.31(t, 1H, *J* = 9.2 Hz, H-4′ phenyl), 7.40(t, 1H, *J* = 7.2 Hz, H-4, *N*-phenyl), 7.50(dt, 4H, *J* = 8.0 Hz, *J* = 2.8 Hz, H-3, H-5, H-3′, H-5′), 7.70(d, 1H, *J* = 7.2 Hz, H-2′), 7.75 (d, 1H, *J* = 7.2 Hz, H-6′), 7.85(d, *J* = 8.0 Hz, 2H, H-2), 7.90 (d, *J* = 8.0 Hz, 2H, H-6), 8.34(s, 1H, NH-imine exchangeable by D_2O, 78%), 8.48(s, 1H, 5-H pyrimidine-2-amine, 22%), 8.98(s, 1H, pyrazole-H). ^{13}C NMR (100 MHz, DMSO-d_6): δ 56.0(*m*-methoxy), 60.1(*p*-methoxy), 104.0(C-2, C-6 trimethoxyphenyl), 105.7(C-5 pyrimidine), 118.7(C-4 pyrazole), 127.5(C-2, C-6), 128.0(C-4), 128.3(C-2′, C-6′), 128.4(C-1 trimethoxyphenyl), 128.6(C-4′), 128.7(C-3′, C-5′), 129.0(C-3, C-5), 129.5(C-3 pyrazole), 133.0(C-1′), 139.1(C-1), 142.0(C-4 trimethoxyphenyl), 151.0(C-5 pyrazole), 152.8 (C═NH), 153.0(C-3, C-5 trimethoxyphenyl), 163.8(C-4 pyrimidine), 164.0(C-6 pyrimidine). LC-MS/MS *m*/*z* (ESI): 480.15 $[M+H]^+$. Anal. Calc. for $C_{28}H_{25}N_5O_3$ (MW; 479.54) calculated %; C: 70.13, H: 5.26, N: 14.60. Found %; C: 70.10, H: 5.29, N: 14.57.

*4.1.3. Procedure for the Synthesis of 1′,3′-Diphenyl-5-(3,4,5-trimethoxyphenyl)-3,4-dihydro-1′H,2H-3,4′-bipyrazole Derivatives **6a** and **6b**.* A mixture of chalcone **4** (0.4 g, 0.001 mol) and hydrazine hydrate 98% or phenyl hydrazine (0.002 mol) in absolute ethanol (10 mL) was refluxed for 4 h. The formed precipitate was filtered, dried, and recrystallized from ethanol to give the corresponding compounds **6a** and **6b**.

*4.1.3.1. 1′,3′-Diphenyl-5-(3,4,5-trimethoxyphenyl)-3,4-dihydro-1′H,2H-3,4′-bipyrazole (**6a**).* Yellow crystals, mp 141−143 °C, yield (85%), IR (KBr, ν, cm^{-1}): 3425(NH), 3061 (CH-aromatic), 2844−2927 (CH-aliphatic), 1593 (C═N), 1126 (C−O aliphatic ether). ^{1}H NMR (400 MHz, DMSO-d_6): δ 3.01(dd, 1H, *J* = 10.80 Hz, *J* = 4.8 Hz, H-4 pyrazoline), 3.34(s, 3H, *p*-methoxy), 3.84(dd, 1H, *J* = 10.80 Hz, *J* = 4.8 Hz, H-4 pyrazoline), 3.80(s, 6H, *m*-methoxy), 4.98(t, 1H, *J* = 10.80 Hz,H-5 pyrazoline), 6.93(s, 2H, H-2, H-6 trimethoxyphenyl), 7.31(dt, 1H, *J* = 7.2 Hz, *J* = 4.0 Hz, H-4′ phenyl), 7.42(t, 1H, *J*= 7.2 Hz, H-4, *N*-phenyl), 7.50(t, 4H, *J* = 6.8 Hz,H-3, H-5, H-3′, H-5′), 7.78(d, 2H, *J* = 7.60 Hz, H-2′, H-6′), 7.89(dt, 2H, *J* = 8.0 Hz, *J* = 3.6 Hz, H-2, H-6), 8.55(s, 1H, pyrazole-H), 8.69(s, 1H, NH exchangeable by D_2O). ^{13}C NMR (100 MHz, DMSO-d_6): δ 40.1(C-4 pyrazoline), 46.2(C-5 pyrazoline), 55.9(*m*-methoxy), 60.1(*p*-methoxy), 103.0(C-2, C-6 trimethoxyphenyl), 118.2(C-4 pyrazole), 127.9(C-2, C-6), 128.0(C-5 pyrazole), 128.2(C-4, C-2′, C-6′), 128.4(C-1 trimethoxyphenyl), 128.5(C-4′), 128.6(C-3′, C-5′), 129.0(C-3, C-5), 133.0(C-1′), 138.0(C-1), 139.4(C-4 trimethoxyphenyl), 149.3(C-3 pyrazole), 151.2(C-3 pyrazoline), 153.0(C-3, C-5 trimethoxyphenyl). LC-MS/MS *m*/*z* (ESI): 455.15 $[M + H]^+$. Anal. Calc. for $C_{27}H_{26}N_4O_3$(MW; 454.53) calculated %; C: 71.35, H: 5.77, N: 12.33. Found %; C: 71.31, H: 5.80, N: 12.30.

*4.1.3.2. 1′,2,3′-Triphenyl-5-(3,4,5-trimethoxyphenyl)-3,4-dihydro-1′H,2H-3,4′-bipyrazole (**6b**).* Beige crystals, mp 144−1146 °C, yield (79%), IR (KBr, ν, cm^{-1}): 3060 (CH-aromatic), 2828−2966 (CH-aliphatic), 1595 (C═N), 1124 (C−O aliphatic ether). ^{1}H NMR (400 MHz, DMSO-d_6): δ 3.44(dd, 1H, *J* = 4.8 Hz, *J* = 12.0 Hz, H-4 pyrazoline), 3.70(s, 3H, *p*-methoxy), 3.85(s, 6H, *m*-methoxy), 4.06(dd, 1H, *J* = 12.0 Hz, *J* = 7.2 Hz, H-4 pyrazoline), 5.52(dd, 1H, *J* = 7.2 Hz, *J* = 4.8 Hz H-5 pyrazoline), 6.72(t, 1H, *J* = 7.2 Hz, H-4 *N*-phenylpyrazoline), 6.98(d, 2H, *J* = 8.0 Hz, H-2, H-6 *N*-phenylpyrazoline), 7.05(s, 2H, H-2, H-6 trimethoxyphenyl), 7.14(t, 2H, *J* = 8.0 Hz, H-3, H-5 *N*-phenylpyrazoline), 7.27(t, 1H, *J* = 7.2 Hz, H-4′ phenyl), 7.45(q, 3H, *J* = 7.2 Hz, H-4, H-3, H-5, *N*-phenyl), 7.54(t, 2H, *J* = 8.0 Hz, H-3′, H-5′), 7.83(t, 4H, *J* = 7.2 Hz, H-2, H-6, H-2′, H-6′), 8.31(s, 1H, pyrazole-H). ^{13}C NMR (100 MHz, DMSO-d_6): δ 42.2(C-4 pyrazoline), 49.1(C-3 pyrazoline), 56.0(*m*-methoxy), 60.1(*p*-methoxy), 103.2(C-2, C-6 trimethoxyphenyl), 113.3(C-2″, C-6″), 118.2(C-2, C-6), 118.9(C-4 pyrazole), 123.0(C-4″), 126.4(C-5 pyrazole), 127.0(C-4), 128.0(C-1 trimethoxyphenyl, C-2′, C-6′), 128.3(C-4′), 128.7(C-3′, C-5′), 128.9(C-3, C-5), 129.5(C-3″, C-5″), 132.4(C-1′), 138.4(C-1), 139.2(C-4 trimethoxyphenyl), 144.4(C-1″), 147.7(C-3 pyrazole), 149.4(C-5 pyrazoline), 153.0(C-3, C-5 trimethoxyphenyl). Anal. Calc. for $C_{33}H_{30}N_4O_3$ (MW; 530.63) calculated %; C: 74.70, H: 5.70, N: 10.56. Found %; C: 74.66, H: 5.73, N: 10.52.

*4.1.4. Procedure for the Synthesis of 1-(1′,3′-Diphenyl-5-(3,4,5-trimethoxyphenyl)-3,4-dihydro-1′H,2H-[3,4′-bipyrazol]-2-yl)ethan-1-one (**7**).* A mixture of chalcone **4** (0.4 g, 0.001 mol) and hydrazine hydrate 98% (0.10 mL, 0.002 mol) in glacial acetic acid (10 mL) was refluxed for 4 h. The formed precipitate was filtered, dried, and recrystallized from acetic acid to give the title compound **7**.

Pale white crystals, mp 193−197 °C, yield (83%), IR (KBr, ν, cm^{-1}): 3067 (CH-aromatic), 2834−2994 (CH-aliphatic), 1656 (C═O), 1598 (C═N), 1131 (C−O aliphatic ether). ^{1}H NMR (400 MHz, DMSO-d_6): δ 2.32(s, 3H, CH_3 acyl), 3.70(s, 3H, *p*-methoxy), 3.82(s, 6H, *m*-methoxy), 3.83(dd, 1H, *J* = 6.4 Hz, *J* = 4.8 Hz, H-4 pyrazoline), 3.89(dd, 1H, *J* = 11.6 Hz, *J* = 6.4 Hz, H-4 pyrazoline), 5.69(dd, 1H, *J* = 11.6 Hz, *J* = 4.8 Hz, H-5 pyrazoline), 7.01(s, 2H, H-2, H-6 trimethoxyphenyl), 7.29(t, 1H, *J* = 7.2 Hz, H-4′ phenyl), 7.43(t, 1H, *J* = 7.2 Hz, H-4, *N*-phenyl), 7.47(t, 2H, *J* = 6.8 Hz, H-3, H-5), 7.51(t, 2H, *J* = 7.2 Hz, H-3′, H-5′), 7.81(d, 2H, *J* = 7.2 Hz, H-2′, H-6′), 7.89(d, 2H, *J* = 8.4 Hz, H-2, H-6), 8.33(s, 1H, pyrazole-H), 9.65(s, 1H, NH exchangeable by D_2O). ^{13}C NMR (100 MHz, DMSO-d_6): δ 21.8(C−CH_3), 42.3(C-4 pyrazoline), 52.1(C-3 pyrazoline), 56.0(*m*-methoxy), 60.2(*p*-methoxy), 104.2(C-2, C-6 trimethoxyphenyl), 118.1(C-2, C-6), 123.7(C-4 pyrazole), 126.2(C-5 pyrazole), 126.8(C-4), 128.0(C-1 trimethoxyphenyl, C-2′, C-6′), 128.6(C-4′, C-3′, C-5′), 129.4(C-3, C-5), 132.9(C-1′), 139.1(C-1), 139.2(C-4 trimethoxyphenyl), 149.2(C-3 pyrazole), 152.9(C-3, C-5 trimethoxyphenyl), 154.0(C-5 pyrazoline), 167.5 (C═O). Anal. Calc. for $C_{29}H_{28}N_4O_4$ (MW; 496.57) calculated %; C: 70.15, H: 5.68, N: 11.28. Found %; C: 70.12, H: 5.71, N: 11.25.

4.2. Biological Screening. *4.2.1. In Vitro Antimicrobial Activity. 4.2.1.1. Agar Diffusion Method.* DMSO was purchased from Sigma-Aldrich St. Louis, MA, USA conc. sulfuric acid 95%, and barium chloride was obtained from El-Nasr Pharmaceutical Chemicals Company, Egypt (ADWIC). MRSA and *P. aeruginosa* were obtained from the culture collection of the Department of Microbiology and Immunology, Faculty of Pharmacy, Delta University for Science and

https://doi.org/10.1021/acsomega.3c06936
ACS Omega 2023, 8, 44250−44264

Table 4. Treatment Protocol

group	scarring	ketamine/xylazine	methylprednisolone	MRSA infection	saline	drug dispersion
normal	+	+	+	−	+	−
MRSA group	+	+	+	+	−	−
MRSA/**5c** dispersion	+	+	+	+	−	+

Technology. Nutrient agar, Muller−Hinton, and Cefoxitin discs were obtained from Oxoid, Hampshire, England, and the Resazurin dye was supplied from Sigma-Aldrich Company, UK and was prepared by dissolving 15 mg in 100 mL of distilled water to obtain 0.015%, then vortexed and sterilized by filtration, and stored in a refrigerator at 4 °C.[36]

Bacterial Inoculum Preparation. The Cefoxitin disc diffusion method was used for the identification of MRSA[41] Mueller−Hinton broth (MHB) cultures of the test bacterial organisms, MRSA and *P. aeruginosa* were incubated according to CLSI guidelines, and the optical density at 600 nm was adjusted to 10^8 CFU mL^{-1} (colony forming units/mL) by matching with standard half McFarland solution (0.05 mL of 1.175% of barium chloride + 9.95 mL of 1% of conc. sulfuric acid).[36,42] A sterile cotton swab was dipped into the inoculum suspension, either MRSA or *P. aeruginosa*, streaked over the prepared sterile Mueller−Hinton agar plate, and incubated for 24−48 h at 37 °C.

Determination of the Inhibition Zones. A sterile cork borer or tip, a hole with a diameter of 6−8 mm, was aseptically punched, and a volume (100 μL) of the target compounds dissolved in DMSO at the required concentration (10 mg/mL) was placed into the well in an agar plate seeded with either MRSA or *P. aeruginosa* in triplicates. No inhibition zone was observed with the vehicle alone. The plates were incubated at 37 °C for 24 h, the inhibition zone was measured in millimeters (mm), and compounds that showed an inhibition zone >18 mm were further tested for their minimal inhibitory concentration (MIC).

4.2.1.2. Determination of the Minimal Inhibitory Concentration (MIC). The MICs of compounds **5a−c** were determined using the Resazurin-based 96-well plate microdilution method.[43] The concentration range of the tested compounds and the reference drug levofloxacin in the wells (1−10) was 8−0.015 mg mL^{-1}, which was achieved through serial dilutions. Column 12 contained the medium broth as a negative control to monitor sterility when preparing the plate, while column 11 contained the diluted standardized inoculum as a positive control. The standardized bacterial suspension (0.5 McFarland) was 100-fold diluted in MHB, and 50 μL of the adjusted OD600 bacterial suspension was added to all wells, except column 12, resulting in approximately 5×10^5 CFU mL^{-1} in each well. After incubation for 24 h at 37 °C, Resazurin (0.015%) was added to all wells (30 μL per well) and incubated for an additional 2−4 h at 37 °C until a color change was visible. Each well's growth was contrasted with that positive control. The lowest concentration of the tested compound at which color change occurred was taken as the MIC value. The average of three values was calculated, and that was the MIC, following the CLSI recommendation.

4.2.2. Dihydrofolate Reductase (DHFR) Inhibitory Assay. The inhibitory assay of target compounds against the DHFR enzyme was described in our previous report[44] and conducted as specified in the BioVision manufacturer's protocol, taking TMP as the standard drug instead of methotrexate.[45,46]

4.2.3. In Vivo Antimicrobial Activity. 4.2.3.1. Animals. Adult male Sprague−Dawley rats (200 ± 15 g) were purchased from Delta University for Science and Technology, Gamasa, Egypt. Care and protocols were approved by the Research Ethics Committee (approval number: FPDU 5/2023) and carried out following applicable guidelines and policies.

4.2.3.2. In Vivo Ocular Irritation Test. We examined the degree of eye irritation upon application of the studied **5c** dispersion in saline in rats' eyes as previously described.[47] The criteria for accepting the ocular irritation test included degrees of opacity and ulceration of the corneas, swelling and hyperemia of the iris, redness and discernibility of the conjunctiva, and the openness and edema of lids.

4.2.3.3. Induction of Keratitis. The right eye cornea of each immunocompromised rat was scarred using a 27-gauge needle after anesthesia with an intraperitoneal ketamine (50 mg/kg)-xylazine (10 mg/kg) mixture.[48] The cornea was then pipetted with 0.6% acetylcysteine to break up the tear film and washed with a normal saline solution. Following that, a 10 L suspension containing 5×10^8 CFU of MRSA strain of a clinical isolate from a human corneal ulcer was applied and evenly distributed onto the wounded cornea. Rats' left eyes served as blank eyes and were scarred by the same pattern, but they were not infected.[49]

4.2.3.4. Procedure of the In Vivo Anti-MRSA Evaluation. To induce keratitis, rats were immunocompromised with methylprednisolone (50 mg/kg) for 3 days before infection, the day of infection, and 1 day after infection. The rats were divided into three groups: normal rats served as the normal control group ($n = 6$), untreated rats were infected with MRSA ($n = 8$), and rats were infected with MRSA and treated with compound **5c** dispersion ($n = 8$) (Table 4). Three days after the infection, the administration began. The infection was discovered and confirmed by an ophthalmologist who was unaware of the treatment plan. On the third day after the MRSA infection, the corneas had a visually cloudy appearance. Treatment was continued for another 2 days until the visually cloudy appearance of the corneas was completely reduced in one infected animal of the treatment groups.

4.2.3.5. Haematoxylin and Eosin (H&E) Staining and Calculation of the Inflammation Score. To examine histological inflammation of the eye cornea using H and E staining, formalin-fixed and paraffin-embedded tissue samples were first deparaffinized by using xylene and then rehydrated with a series of ethanol solutions. The samples were stained with hematoxylin solution for 5−10 min, rinsed with tap water, differentiated with 1% acid alcohol, and counterstained with eosin solution for 1−2 min. After the samples were rinsed and dehydrated, they were cleared with xylene and mounted on microscope slides with a coverslip.[50,51] The degree of inflammation was determined by evaluating the presence of immune cells and morphological changes in corneal cells under a microscope. The inflammation was graded based on a scoring system that included 0 for no inflammation, 1 for minimal inflammation, 2 for mild inflammation, 3 for moderate inflammation, and 4 for severe inflammation.

https://doi.org/10.1021/acsomega.3c06936
ACS Omega 2023, 8, 44250−44264

Statistical analysis was carried out using GraphPad Prism software, version 8.0.2 (GraphPad Software Inc., La Jolla, CA, USA). In the statistical analysis of corneal opacity, differences between groups were analyzed using a one-way analysis of variance followed by Tukey as a posthoc test. The mean and standard deviation were used to represent the data. A P value of 0.05 was considered to be statistically significant.

4.3. Molecular Modeling Simulation. Wild-type *S. aureus* DHFR in complex with TMP was retrieved from the Protein Data Bank (PDB ID: 2W9H) at a resolution of 1.48 Å.[52] With their standard geometry, all hydrogen atoms were added to the crystal 3D structure of the protein followed by their energy minimization. Our investigated compounds and TMP were drawn into Marvin Sketch of Marvin suite (http://www.chemaxon.com) to generate the lowest energy conformer. The dock module of MOE (Molecular Operating Environment) version MOE 2019.0102[53] was utilized in docking studies. Our newly synthesized compounds were docked against the rigid binding pocket, the active site of TMP, of the protein using flexible ligand mode. The placement phase generated poses from ligand conformations. The free binding energy of the ligand from a certain pose was calculated using the force field-based scoring function GBVI/WSA ΔG.[54]

■ ASSOCIATED CONTENT

Supporting Information

The Supporting Information is available free of charge at https://pubs.acs.org/doi/10.1021/acsomega.3c06936.

Spectral charts (IR, ^{1}H NMR, ^{13}C NMR, and LC-MS/MS) of some new compounds; resultant 2D and 3D poses and free binding energies from docking (**4**, **5a−c**, **6a,b**, and **7**) against the crystal structure of wild-type *S. aureus* DHFR in complex with TMP (PDB ID: 2W9H) (PDF)

■ AUTHOR INFORMATION

Corresponding Author

Basem Mansour − *Department of Pharmaceutical Chemistry, Faculty of Pharmacy, Delta University for Science and Technology, Gamasa 11152 Dakahlia, Egypt;* orcid.org/0000-0001-6266-8864; Phone: +2 050 277 0140; Email: basem2412@yahoo.com; Fax: +2 050 277 0145

Authors

Magda A. El-Sherbeny − *Department of Pharmaceutical Chemistry, Faculty of Pharmacy, Delta University for Science and Technology, Gamasa 11152 Dakahlia, Egypt; Department of Medicinal Chemistry, Faculty of Pharmacy, University of Mansoura, Mansoura 35516, Egypt;* orcid.org/0000-0001-6415-4664

Fatmah A. M. Al-Omary − *Department of Pharmaceutical Chemistry, College of Pharmacy, King Saud University, Riyadh 11451, Saudi Arabia*

Sameh Saber − *Department of Pharmacology, Faculty of Pharmacy, Delta University for Science and Technology, Gamasa 11152 Dakahlia, Egypt*

Heba A. Ramadan − *Department of Microbiology and Immunology Faculty of Pharmacy, Delta University for Science and Technology, Gamasa 11152 Dakahlia, Egypt*

Ahmed M. El-Baz − *Department of Microbiology and Immunology Faculty of Pharmacy, Delta University for Science and Technology, Gamasa 11152 Dakahlia, Egypt*

Ahmed A. E. Mourad − *Department of Pharmacology and Toxicology, Faculty of Pharmacy, Port Said University, Port Said 42511, Egypt*

Naglaa I. Abdel-Aziz − *Department of Pharmaceutical Chemistry, Faculty of Pharmacy, Delta University for Science and Technology, Gamasa 11152 Dakahlia, Egypt; Department of Medicinal Chemistry, Faculty of Pharmacy, University of Mansoura, Mansoura 35516, Egypt*

Complete contact information is available at: https://pubs.acs.org/10.1021/acsomega.3c06936

Notes

The authors declare no competing financial interest.

■ ACKNOWLEDGMENTS

Our profound appreciation goes to the Drug Discovery and Development unit, Faculty of Pharmacy, Delta University for Science and Technology, for providing us with some chemicals and Holding Company for Biological Products and Vaccines (VACSERA), Cairo, Egypt, for performing the enzyme inhibitory assay.

■ REFERENCES

(1) Kovalev, I. S.; Zyryanov, G. V.; Santra, S.; Majee, A.; Varaksin, M. V.; Charushin, V. N. Folic Acid Antimetabolites (Antifolates): A Brief Review on Synthetic Strategies and Application Opportunities. *Molecules* **2022**, *27* (19), 6229.

(2) Zhou, W.; Scocchera, E. W.; Wright, D. L.; Anderson, A. C. Antifolates as effective antimicrobial agents: new generations of trimethoprim analogs. *MedChemComm* **2013**, *4* (6), 908−915.

(3) Pedrola, M.; Jorba, M.; Jardas, E.; Jardi, F.; Ghashghaei, O.; Viñas, M.; Lavilla, R. Multicomponent reactions upon the known drug trimethoprim as a source of novel antimicrobial agents. *Front. Chem.* **2019**, *7*, 475.

(4) Kumar, A.; Singh, K. A.; Thareja, S.; Kumar, P. A Review of Pyridine and Pyrimidine Derivatives as Anti-MRSA Agents. *Anti-Infect. Agents.* **2023**, *21*, 18−40.

(5) Nanjundaswamy, S.; Bindhu, S.; Arun Renganathan, R.; Nagashree, S.; Karthik, C.; Mallu, P.; Ravishankar Rai, V. Design, synthesis of pyridine coupled pyrimidinone/pyrimidinthione as anti-MRSA agent: Validation by molecular docking and dynamics simulation. *J. Biomol.* **2022**, *40*, 12106.

(6) Wróbel, A.; Maliszewski, D.; Baradyn, M.; Drozdowska, D. Trimethoprim: An old antibacterial drug as a template to search for new targets. Synthesis, biological activity and molecular modeling study of novel trimethoprim analogs. *Molecules* **2020**, *25* (1), 116.

(7) Dailidė, M.; Tumkevičius, S. Synthesis of novel 2, 4-diamino-6-(arylaminomethyl) thieno [2, 3-d] pyrimidines as potential antifolates. *Chemija* **2022**, *33* (3), 97−101, DOI: 10.6001/chemija.v33i3.4752.

(8) Sköld, O. Resistance to trimethoprim and sulfonamides. *Vet. Res.* **2001**, *32* (3−4), 261−273.

(9) Fernández-Villa, D.; Aguilar, M. R.; Rojo, L. Folic acid antagonists: antimicrobial and immunomodulating mechanisms and applications. *Int. J. Mol. Sci.* **2019**, *20* (20), 4996.

(10) Hişmioğullari, Ş. E.; Yarsan, E. Spectrophotometric determination and stability studies of sulfamethoxazole and trimethoprim in oral suspension by classical least square calibration method. *Hacettepe Univ. J. Fac. Pharm.* **2009**, *2*, 95−104.

(11) Huang, L.; Chen, X.; Xu, H.; Sun, L.; Li, C.; Guo, W.; Xiang, L.; Luo, G.; Cui, Y.; Lu, B. Clinical features, identification, antimicrobial resistance patterns of Nocardia species in China: 2009−2017. *Diagn. Microbiol. Infect. Dis.* **2019**, *94* (2), 165−172.

(12) Liu, C.; Bayer, A.; Cosgrove, S. E.; Daum, R. S.; Fridkin, S. K.; Gorwitz, R. J.; Kaplan, S. L.; Karchmer, A. W.; Levine, D. P.; Murray, B. E.; Rybak, M. J.; Talan, D. A.; Chambers, H. F. Clinical Practice

Guidelines by the Infectious Diseases Society of America for the Treatment of Methicillin-Resistant Staphylococcus aureus Infections in Adults and Children. *Clin. Infect. Dis.* **2011**, *52* (3), e18−e55.
(13) Lombardo, M. N.; G-Dayanandan, N.; Wright, D. L.; Anderson, A. C. Crystal structures of trimethoprim-resistant DfrA1 rationalize potent inhibition by propargyl-linked antifolates. *ACS. Infect. Dis.* **2016**, *2* (2), 149−156.
(14) Wróbel, A.; Arciszewska, K.; Maliszewski, D.; Drozdowska, D. Trimethoprim and other nonclassical antifolates an excellent template for searching modifications of dihydrofolate reductase enzyme inhibitors. *J. Antibiot.* **2020**, *73* (1), 5−27.
(15) B'Bhatt, H.; Sharma, S. Synthesis and antimicrobial activity of pyrazole nucleus containing 2-thioxothiazolidin-4-one derivatives. *Arab. J. Chem.* **2017**, *10*, S1590−S1596.
(16) Abunada, N. M.; Hassaneen, H. M.; Kandile, N. G.; Miqdad, O. A. Synthesis and antimicrobial activity of some new pyrazole, fused pyrazolo [3, 4-d]-pyrimidine and pyrazolo [4, 3-e][1, 2, 4]-triazolo [1, 5-c] pyrimidine derivatives. *Molecules* **2008**, *13*, 1501−1517.
(17) Sharma, P. K.; Chandak, N.; Kumar, P.; Sharma, C.; Aneja, K. R. Synthesis and biological evaluation of some 4-functionalized-pyrazoles as antimicrobial agents. *Eur. J. Med. Chem.* **2011**, *46*, 1425−1432.
(18) Desai, N. C.; Rajpara, K. M.; Joshi, V. V. Synthesis of pyrazole encompassing 2-pyridone derivatives as antibacterial agents. *Bioorg. Med. Chem. Lett.* **2013**, *23*, 2714−2717.
(19) Verma, R.; Verma, S. K.; Rakesh, K. P.; Girish, Y. R.; Ashrafizadeh, M.; Sharath Kumar, K. S.; Rangappa, K. S. pyrazole-based analogs as potential antibacterial agents against methicillin-resistance staphylococcus aureus (MRSA) and its SAR elucidation. *Eur. J. Med. Chem.* **2021**, *212*, No. 113134.
(20) A Alam, M. Antibacterial pyrazoles: tackling resistant bacteria. *Future Med. Chem.* **2022**, *14* (5), 343−362.
(21) Xu, L.-L.; Zheng, C.-J.; Sun, L.-P.; Miao, J.; Piao, H.-R. Synthesis of novel 1, 3-diaryl pyrazole derivatives bearing rhodanine-3-fatty acid moieties as potential antibacterial agents. *Eur. J. Med. Chem.* **2012**, *48*, 174−178.
(22) Ahmad, A.; Husain, A.; Khan, S. A.; Mujeeb, M.; Bhandari, A. Synthesis, antimicrobial and antitubercular activities of some novel pyrazoline derivatives. *J. Saudi Chem. Soc.* **2016**, *20* (5), 577−584.
(23) Yahya, G.; Ebada, A.; Khalaf, E. M.; Mansour, B.; Nouh, N. A.; Mosbah, R. A.; Saber, S.; Moustafa, M.; Negm, S.; El-Sokkary, M. M. Soil-associated Bacillus species: A reservoir of bioactive compounds with potential therapeutic activity against human pathogens. *Microorganisms* **2021**, *9* (6), 1131.
(24) Kalavathy, C. M.; Parmar, P.; Ramalingam, M. K.; Kaliamurthy, J.; Jesudasan, C. N.; Thomas, P. A. Trimethoprim− sulphamethoxazole therapy in Nocardia keratitis. *Clinical & Experimental Ophthalmology* **2004**, *32* (4), 424−428.
(25) Resnikoff, S.; Pascolini, D.; Etya'Ale, D.; Kocur, I.; Pararajasegaram, R.; Pokharel, G. P.; Mariotti, S. P. Global data on visual impairment in the year 2002. *Bull. W. H. O.* **2004**, *82* (11), 844−851.
(26) Ramadan, E. S.; Sharshira, E. M.; El Sokkary, R. I.; Morsy, N. Synthesis and antimicrobial evaluation of some heterocyclic compounds from 3-aryl-1-phenyl-1 H-pyrazole-4-carbaldehydes. *Zeitschrift für Naturforschung B* **2018**, *73*, 389−397.
(27) Brahmbhatt, D.; Kaneria, A. R.; Patel, A. K.; Patel, N. H. Synthesis and antimicrobial screening of some 3-[4-(3-aryl-1-phenyl-1H-pyrazol-4-yl)-6-aryl-pyridin-2-yl] and 4-methyl-3-phenyl-6-[4-(3-aryl-1-phenyl-1H-pyrazol-4-yl)-6-aryl-pyridin-2-yl] coumarins. *Indian J. Chem.* **2010**, *49B*, 971−977. http://nopr.niscpr.res.in/handle/123456789/9935.
(28) Amer, A.; Ramses, N.; Mahgoub, S. Synthesis, reactions and antitumor activity of certain 1, 3-diphenylpyrazole-4-carboxaldehyde derivatives. *Egypt. J. Chem.* **2018**, *61*, 51−65.
(29) Thirunarayanan, G.; Sekar, K. Solvent-free one-pot cyclization and acetylation of chalcones: Synthesis of some 1-acetyl pyrazoles and spectral correlations of 1-(3-(3,4-dimethylphenyl)-5-(substituted phenyl)-4,5-dihydro-1H-pyrazole-1-yl) ethanones. *J. Saudi Chem. Soc.* **2016**, *20*, 661−672.
(30) Magaldi, S.; Mata-Essayag, S.; Hartung de Capriles, C.; Perez, C.; Colella, M. T.; Olaizola, C.; Ontiveros, Y. Well diffusion for antifungal susceptibility testing. *Int. J. Infect Dis* **2004**, *8* (1), 39−45.
(31) Valgas, C.; Souza, S. M. d.; Smânia, E. F. A.; Smânia, A. Screening methods to determine antibacterial activity of natural products. *Braz. J. Microbiol.* **2007**, *38*, 369−380.
(32) Sihotang, T. S. U.; Widodo, A. D. W.; Endraswari, P. D. Effect of Ciprofloxacin, levofloxacin, and ofloxacin on Pseudomonas aeruginosa: A case control study with time kill curve analysis. *Ann. Med. Surg.* **2022**, *82*, No. 104674.
(33) Zhang, G.-F.; Zhang, S.; Pan, B.; Liu, X.; Feng, L.-S. 4-Quinolone derivatives and their activities against Gram positive pathogens. *Eur. J. Med. Chem.* **2018**, *143*, 710−723.
(34) Gao, C.; Fan, Y.-L.; Zhao, F.; Ren, Q.-C.; Wu, X.; Chang, L.; Gao, F. Quinolone derivatives and their activities against methicillin-resistant Staphylococcus aureus (MRSA). *Eur. J. Med. Chem.* **2018**, *157*, 1081−1095.
(35) Cruickshank, R.; Duguid, J. P.; Marmion, B. P.; Swain, R. H. A. *Medical microbiology: the practice of medical microbiology*; 12 ed.; Churchill Livingstone: Edinburgh, vol 2. 1975.
(36) Elshikh, M.; Ahmed, S.; Funston, S.; Dunlop, P.; McGaw, M.; Marchant, R.; Banat, I. M. Resazurin-based 96-well plate microdilution method for the determination of minimum inhibitory concentration of biosurfactants. *Biotechnol. Lett.* **2016**, *38*, 1015−1019.
(37) El-Gizawy, S. A.; Nouh, A.; Saber, S.; Kira, A. Y. Deferoxamine-loaded transfersomes accelerates healing of pressure ulcers in streptozotocin-induced diabetic rats. *J. Drug Delivery Sci. Technol.* **2020**, *58*, No. 101732.
(38) Bernard, M.; Hulley, E.; Molenda, H.; Stochla, K.; Wrzeciono, U. Azoles. 17. Beta-(4-pyrazol)acrylic and propionic acids and their anti-inflammatory activity. *Pharmazie* **1986**, *41* (8), 560−562.
(39) Kira, M.; Abdel-Rahman, M.; Gadalla, K. The Vilsmeier-Haack reaction-III cyclization of hydrazones to pyrazoles. *Tetrahedron Lett.* **1969**, *10* (2), 109−110.
(40) Prakash, O.; Pannu, K.; Kumar, A. Synthesis of some new 2-(3-aryl-1-phenyl-4-pyrazolyl)-benzoxazoles using hypervalent iodine mediated oxidative cyclization of Schiff's bases. *Molecules* **2006**, *11* (1), 43−48.
(41) Skov, R.; Smyth, R.; Larsen, A.; Frimodt-Møller, N.; Kahlmeter, G. Evaluation of Cefoxitin 5 and 10 μg discs for the detection of methicillin resistance in staphylococci. *J. Antimicrob. Chemother.* **2005**, *55* (2), 157−161.
(42) El-Baz, A. M.; Yahya, G.; Mansour, B.; El-Sokkary, M.; Alshaman, R.; Alattar, A.; El-Ganiny, A. M. The Link between Occurrence of Class I Integron and Acquired Aminoglycoside Resistance in Clinical *MRSA* Isolates. *Antibiotics* **2021**, *10* (5), 488.
(43) Wikler, M. A. Methods for dilution antimicrobial susceptibility tests for bacteria that grow aerobically: approved standard. *CLSI (NCCLS)* **2006**, *26*, M7-A7.
(44) Omar, A. M.; Alswah, M.; Ahmed, H. E. A.; Bayoumi, A. H.; El-Gamal, K. M.; El-Morsy, A.; Ghiaty, A.; Afifi, T. H.; Sherbiny, F. F.; Mohammed, A. S.; Mansour, B. A. Antimicrobial screening and pharmacokinetic profiling of novel phenyl-[1,2,4]triazolo[4,3-a]-quinoxaline analogues targeting DHFR and E. coli DNA gyrase B. *Bioorg. Chem.* **2020**, *96*, No. 103656.
(45) Riyadh, S. M.; El-Motairi, S. A.; Ahmed, H. E.; Khalil, K. D.; Habib, E. S. E. Synthesis, biological evaluation, and molecular docking of novel thiazoles and [1, 3, 4] thiadiazoles incorporating sulfonamide group as DHFR Inhibitors. *Chem. Biodivers.* **2018**, *15* (9), No. e1800231.
(46) Widemann, B. C.; Balis, F. M.; Adamson, P. C. Dihydrofolate reductase enzyme inhibition assay for plasma methotrexate determination using a 96-well microplate reader. *Clin. Chem.* **1999**, *45* (2), 223−228.
(47) Hosny, K. M.; Rizg, W. Y.; Alkhalidi, H. M.; Abualsunun, W. A.; Bakhaidar, R. B.; Almehmady, A. M.; Alghaith, A. F.; Alshehri, S.;

https://doi.org/10.1021/acsomega.3c06936
ACS Omega 2023, 8, 44250−44264

El Sisi, A. M. J. D. D. Nanocubosomal based in situ gel loaded with natamycin for ocular fungal diseases: development, optimization, *in-vitro*, and *in-vivo* assessment. *Drug Delivery* **2021**, *28* (1), 1836−1848.
(48) Nasr, M.; Teiama, M.; Ismail, A.; Ebada, A.; Saber, S. In vitro and in vivo evaluation of cubosomal nanoparticles as an ocular delivery system for fluconazole in treatment of keratomycosis. *Drug Delivery and Translational Research* **2020**, *10* (6), 1841−1852.
(49) El-Telbany, M.; Mohamed, A. A.; Yahya, G.; Abdelghafar, A.; Abdel-Halim, M. S.; Saber, S.; Alfaleh, M. A.; Mohamed, A. H.; Abdelrahman, F.; Fathey, H. A.; Ali, G. H.; Abdel-Haleem, M. Combination of Meropenem and Zinc Oxide Nanoparticles; Antimicrobial Synergism, Exaggerated Antibiofilm Activity, and Efficient Therapeutic Strategy against Bacterial Keratitis. *Antibiotics* **2022**, *11* (10), 1374.
(50) Cavalu, S.; Sharaf, H.; Saber, S.; Youssef, M. E.; Abdelhamid, A. M.; Mourad, A. A. E.; Ibrahim, S.; Allam, S.; Elgharabawy, R. M.; El-Ahwany, E.; Amin, N. A.; Shata, A.; Eldegla, M.; Atef, M.; Aboraya, M.; Mohamed, M.; Anz, N.; Elmotelb, D. A.; Gabr, F.; Elzablawy, D.; Hamada, M.; Yehia, A.; Osama, D.; Mohammed, O. A. Ambroxol, a mucolytic agent, boosts HO-1, suppresses NF-κB, and decreases the susceptibility of the inflamed rat colon to apoptosis: A new treatment option for treating ulcerative colitis. *Faseb J.* **2022**, *36* (9), No. e22496.
(51) Youssef, M. E.; El-Azab, M. F.; Abdel-Dayem, M. A.; Yahya, G.; Alanazi, I. S.; Saber, S. Electrocardiographic and histopathological characterizations of diabetic cardiomyopathy in rats. *Environ. Sci. Pollut. Res.* **2022**, *29* (17), 25723−25732.
(52) Heaslet, H.; Harris, M.; Fahnoe, K.; Sarver, R.; Putz, H.; Chang, J.; Subramanyam, C.; Barreiro, G.; Miller, J. R. Structural comparison of chromosomal and exogenous dihydrofolate reductase from Staphylococcus aureus in complex with the potent inhibitor trimethoprim. *Proteins: Struct., Funct., Bioinf.* **2009**, *76* (3), 706−717.
(53) Molecular Operating Environment (MOE). *Chemical Computing Group Inc.: 1010 Sherbooke St. West*; Suite# 910, 2008, Montreal, QC, Canada.
(54) Labute, P. The generalized Born/volume integral implicit solvent model: estimation of the free energy of hydration using London dispersion instead of atomic surface area. *J. Comput. Chem.* **2008**, *29* (10), 1693−1698.

https://doi.org/10.1021/acsomega.3c06936
ACS Omega 2023, 8, 44250−44264